Bistatic SAR Processing and Experiments

Ingo Walterscheid, Joachim H. G. Ender, *Senior Member, IEEE*,
Andreas R. Brenner, and Otmar Loffeld, *Senior Member, IEEE*

***Abstract*—Bistatic synthetic aperture radar (SAR) uses a separated transmitter and receiver flying on different platforms to achieve benefits like exploitation of additional information contained in the bistatic reflectivity of targets, reduced vulnerability for military applications, forward-looking SAR imaging, or increased radar cross section. Besides technical problems such as synchronization of the oscillators, involved adjustment of transmit pulse versus receive gate timing, antenna pointing, flight coordination, and motion compensation, the development of a bistatic focusing algorithm is still in progress and not sufficiently solved. As a step to a numerically efficient processor, this paper presents a bistatic range migration algorithm for the translationally invariant case, where transmitter and receiver have equal velocity vectors. In this paper, the algorithm was successfully applied to simulated and real bistatic data. The real bistatic data have been acquired with the Forschungsgesellschaft für Angewandte Naturwissenschaften (FGAN)'s X-band SAR systems, namely the Airborne Experimental Radar II and the Phased Array Multifunctional Imaging Radar, in October 2003.**

***Index Terms*—Bistatic SAR, bistatic SAR experiments, range migration algorithm, synthetic aperture radar (SAR).**

I. Introduction

THE INTEREST in bistatic synthetic aperture radar (SAR) has rapidly increased in the last years. This is based on the specific advantages of bistatic SAR configurations in comparison with monostatic systems like the increased information content of bistatic SAR data with regard to feature extraction and classification. This could be worthwhile, e.g., for topographic features, surficial deposits, and drainage, to show the relationships that occur between forest, vegetation, and soils. This provides important information for land classification and land-use management. Also, agriculture monitoring, soils mapping, and archaeological investigations could benefit from bistatic SAR imaging.

Even for objects that show a low radar cross section (RCS) in monostatic SAR images, one can find distinct bistatic angles to increase their RCS to make these objects visible in the final SAR image. On the other hand, especially urban areas are affected by strong reflections due to the dihedral and polyhedral effects, which can be reduced by using different positions for the transmitter and receiver, which means a bistatic SAR constellation. The result is a more homogeneous SAR image in contrast to the monostatic case.

Manuscript received September 30, 2005; revised February 17, 2006. This work was supported by the German Federal Ministry of Defense (BMVg) and the Federal Office of Technology and Procurement (BWB).

I. Walterscheid, J. H. G. Ender, and A. R. Brenner are with the Research Institute for High Frequency Physics and Radar Techniques (FHR), Forschungsgesellschaft für Angewandte Naturwissenschaften, 53343 Wachtberg, Germany (e-mail: walterscheid@fgan.de; ender@fgan.de; brenner@fgan.de).

O. Loffeld is with the Center of Sensorsystems (ZESS), University of Siegen, 57068 Siegen, Germany (e-mail: loffeld@zess.uni-siegen.de).

Digital Object Identifier 10.1109/TGRS.2006.881848

Remote sensing with bistatic SAR systems can be realized with different platform pairs. For example, future bistatic SAR applications could use small "receive-only" SAR systems mounted on airplanes, unmanned aerial vehicles (UAVs), or mountains in conjunction with a satellite as transmitter, or both the transmitter and receiver could be mounted on airplanes like in the bistatic experiments described in this paper. In any a case, the space–time synchronization of the antenna footprints is a big problem. The key element to achieve an overlap of the footprints is the electronically steerable phased array antennas. The advantage of these antennas is the possibility to track the antenna beam very quickly.

This paper presents a bistatic range migration algorithm for the special case of equal velocity vectors of transmitter and receiver. A first approach was introduced in [1] for a two-dimensional (2-D) geometry. In [2], another bistatic range migration algorithm for a three-dimensional (3-D) geometry was proposed, where the SAR image is directly reconstructed in the ground plane. The processor is not optimum in the sense of the monostatic range migration processor, but the degradation is negligible for wide ranges of geometrical parameters. The advantage of such a Fourier-based processor is its numerically efficiency.

A further approach of a range migration processor [3] is very similar to [2] and [4], but it uses a physical reference and approximates the linear phase term by a Taylor series.

Another type of a bistatic SAR processor is presented in [5] and [6]. In both approaches, the bistatic processing will be done by quasi-monostatic processing after initially convolving the raw data with a bistatic deformation term.

In the next section, we introduce the bistatic geometry and the bistatic slant range histories. In Section III, a signal model for bistatic received signals is presented. Then, the bistatic range migration algorithm will be explained in detail in Section IV. A slightly different approach for a bistatic range migration algorithm based on [3] is presented in Section V. The minor differences to the approach in Section IV will be pointed out. In Section VI, the validity of the algorithm is checked with simulated bistatic data, and in Section VII, we test the algorithm with real bistatic data from an airborne SAR experiment with X-band SAR systems, namely the Airborne Experimental Radar II (AER-II) and the Phased Array Multifunctional Imaging Radar (PAMIR). Also, a bistatic image processed by a time-domain processor will be presented at the end of this paper. Such a processor can be used for general bistatic constellations and offers the best focusing results but suffers from its large computational load.

II. Geometrical Relations

The complexity of bistatic geometrical constellations varies from the special case of a monostatic geometry, where

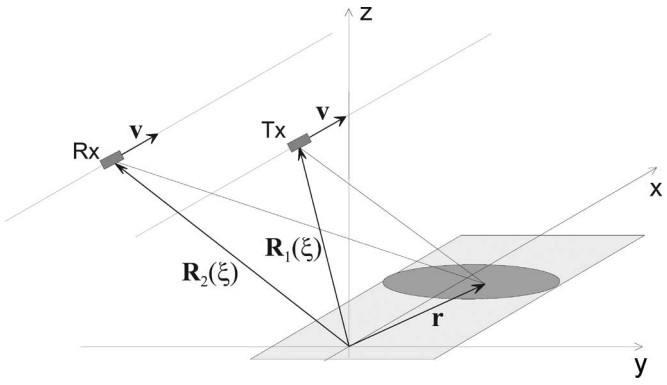

Fig. 1. Bistatic geometry.

transmitter and receiver are located at the same position, to a general bistatic constellation, where transmitter and receiver have arbitrary velocity vectors. In this paper, we restrict to the so-called spatial invariant case, in which the velocity vectors of transmitter and receiver are equal (see Fig. 1). There are two special cases for such a configuration: 1) the "tandem configuration," in which the transmitter and receiver are travelling along the same path with constant and equal velocities, and 2) the "across-track configuration," in which the transmitter and receiver are travelling along different but parallel tracks, where the coordinates in the direction of motion coincide.

In the direction of motion, the received signals are Nyquist sampled, so that no Doppler ambiguities are expected, and the range swath width was adapted in such a way that no range ambiguities occur. Because the PRF is higher than the Nyquist sampling rate, we prefer to use a continuous signal model instead of discrete values.

The scene coordinate system in Fig. 1 is arranged in such a way that the common velocity vector $\mathbf{v}$ points to the direction of the x axis. The positions of the transmit (index 1) and receive (index 2) antenna phase centers are denoted by $\mathbf{R}_1(\xi)$ and $\mathbf{R}_2(\xi)$, where ξ is a path parameter in spatial units. The position of the antenna phase centers can then be expressed by the following vector equation of a straight line parallel to the x axis:

$$\mathbf{R}_i(\xi) = \mathbf{R}_i^{(0)} + (\xi, 0, 0)^t \tag{1}$$

where $\mathbf{R}_i^{(0)}$ is the vector to the sensor position at $\xi = 0$.

Furthermore, we regard an arbitrary point scatterer in the xy plane at the position $\mathbf{r} = (x, y, 0)^t$. Then, the bistatic range history is defined by the sum of the transmit $R_1(\xi; \mathbf{r})$ and receive range history $R_2(\xi; \mathbf{r})$, i.e.,

$$\begin{aligned} R(\xi; \mathbf{r}) &= R_1(\xi; \mathbf{r}) + R_2(\xi; \mathbf{r}) \\ &= |\mathbf{R}_1(\xi) - \mathbf{r}| + |\mathbf{R}_2(\xi) - \mathbf{r}|. \end{aligned} \tag{2}$$

The bistatic range history loses its hyperbolic form, which is known of the monostatic case, because the sum of two hyperbolas is no longer a hyperbola. The shape is flattened, and therefore, we speak of a so-called flat-top parabola.

Throughout this paper, we use the exact expression (2) for the bistatic range history, and we will not restrict to range approximations because we intend to apply the processor for high-resolution imaging with large processing angles and large relative swath width for which range approximations, for instance by a polynomial of order two, are no longer valid.

III. Signal Model

Let the transmit RF signal be denoted by $s_t(t)$ and its spectrum by $S_t(f)$, which covers a certain frequency band $[f_1, \ldots, f_2]$ corresponding to a band of range wavenumbers $[k_{r,1}, \ldots, k_{r,2}]$ with $k_r = 2\pi f/c$, where c is the velocity of light. The receive RF signal $s_r(\xi, t; \mathbf{r})$ from a point scatterer at position $\mathbf{r}$ and platform position ξ is a time-delayed version of the transmit RF signal $s_t(t)$, i.e.,

$$s_r(\xi, t; \mathbf{r}) = a(\mathbf{r}) s_t(t - t_0) w(\xi; \mathbf{r}) \tag{3}$$

where $a(\mathbf{r})$ is the complex reflectivity of a point scatterer, $t_0 = R(\xi; \mathbf{r})/c$ is the signal time delay with respect to the bistatic range, and $w(\xi; \mathbf{r})$ is a window function, which comprises the effects of the two antenna patterns and the bistatic radar equation. In (3), we are implicitly making the "start–stop" approximation, i.e., we are assuming that the transmit and receive antenna are stationary while the pulse is transmitted and received. This is a good approximation because the antenna speed is so much slower than the speed of propagation of the electromagnetic signals.

If the received signal is transformed to spectral domain and inversely filtered over the signal bandwidth, we obtain the spectrum of the normalized compressed range signal at azimuth position ξ, i.e.,

$$S_r(\xi, f; \mathbf{r}) = a(\mathbf{r}) e^{-j2\pi f t_0} w(\xi; \mathbf{r}). \tag{4}$$

For reasons of clearness, we have skipped the derivation of the normalized compressed range signal. These transformations are common practice and can be looked up, for instance, in [7].

In a next step, the range frequency variable f is substituted by the range wavenumber k_r, i.e.,

$$S_r(\xi, k_r; \mathbf{r}) = a(\mathbf{r}) e^{-jk_r R(\xi; \mathbf{r})} w(\xi; \mathbf{r}). \tag{5}$$

Now, we look for a signal model with a reflectivity distribution $a(\mathbf{r})$, which is assumed to be restricted to the xy plane. Then, we obtain the final signal model by the superposition of the individual contributions of (5), i.e.,

$$Z(\xi, k_r) = \iint e^{-jk_r R(\xi; x, y)} w(\xi; x, y) a(x, y) dx\, dy. \tag{6}$$

IV. Bistatic Range Migration Algorithm

A. Outline of the Algorithm

A flowchart of the bistatic range migration processor is presented in Fig. 2. In the preprocessing step, the range compression is performed. For this, the knowledge of the transmitted waveform is necessary. There are different possibilities to obtain the transmitted signal: 1) you can use the waveform, which is generated at the transmitter; 2) you can use the received direct signal from the transmitter if the receiver platform is within the transmit beam; or 3) you can extract the waveform from the raw data if strong point reflectors are available. Furthermore, an azimuth resampling of the data from the (T, k_r) domain to the (ξ, k_r) domain is necessary if ξ is not a linear function

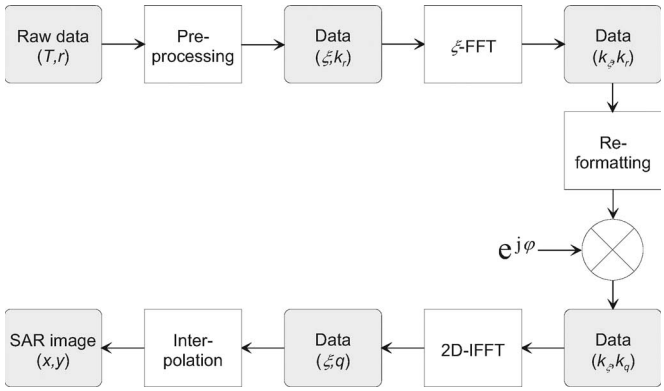

Fig. 2. Range migration algorithm.

of the slow time T. Then, a Fourier transform to the (k_ξ, k_r) domain follows. The next two steps are a kind of a generalized Stolt interpolation: 1) the data will be resampled to the (k_ξ, k_q) domain, where the meaning of k_q will be explained later; and 2) the data will be multiplied by a phasor. It follows a 2-D inverse Fourier transform to the (ξ, q) domain, and finally, we have to resample the image to the xy plane.

B. Variable Transformation

Due to the assumption of translational invariant configurations, the range history $R(\xi; x, y)$ and the radar signal depend only on $\xi' = \xi - x$. Furthermore, the spatial variable y is expressed by a new variable q. The mapping is done by a strict monotonic continuous bijective function $f : y = f(q)$. Our aim is to reconstruct the reflectivity in dependence on the new variable $q : \tilde{a}(x, q) = a(x, f(q))$. The range and window function are replaced by the following expressions:

$$\tilde{R}(\xi'; q) := R\left(\xi; x, f(q)\right) \tag{7}$$
$$\tilde{w}(\xi'; q) := w\left(\xi; x, f(q)\right). \tag{8}$$

By means of these new variables, the signal model is given by

$$Z(\xi, k_r) = \iint e^{-jk_r \tilde{R}(\xi';q)} \tilde{w}(\xi'; q)\tilde{a}(x, q)dx\, dq. \tag{9}$$

C. Fourier Transform in Flight Direction

After applying a Fourier transform to the first variable of $Z(\xi, k_r)$, where $\xi = x + \xi'$, we obtain

$$\begin{aligned} Z(k_\xi, k_r) &= \iiint e^{-jk_r \tilde{R}(\xi';q) - jk_\xi(x+\xi')} \\ &\quad \cdot \tilde{w}(\xi'; q)\tilde{a}(x, q)dx\, dq\, d\xi' \qquad (10) \\ &= \iiint e^{-jk_r \tilde{R}(\xi';q) - jk_\xi \xi'} \\ &\quad \cdot e^{-jk_\xi x} \tilde{w}(\xi'; q)\tilde{a}(x, q)dx\, dq\, d\xi'. \qquad (11) \end{aligned}$$

This equation can be simplified as follows:

$$Z(k_\xi, k_r) = \iint e^{-jk_r \tilde{R}(\xi';q) - jk_\xi \xi'} \tilde{w}(\xi'; q)\tilde{A}(k_\xi, q)dq\, d\xi' \tag{12}$$

where

$$\tilde{A}(k_\xi, q) = \int \tilde{a}(x, q)e^{-jk_\xi x}\, dx \tag{13}$$

is the Fourier transform of the reflectivity distribution $\tilde{a}(x, q)$ in the first dimension.

D. Application of the Principle of Stationary Phase

To simplify (12), we apply the principle of stationary phase. The phase function is given by

$$\begin{aligned} \varphi(k_r, k_\xi; \xi, q) &= -k_r \tilde{R}(\xi; q) - k_\xi \xi \\ &= -k_r \left(\tilde{R}(\xi; q) - C\xi\right) \qquad (14) \end{aligned}$$

where $C = -k_\xi / k_r$. Because only the term in brackets depends on ξ, we only need to determine the points of stationary phase of the function $F(\xi, C, q)$, i.e.,

$$F(\xi, C, q) = \tilde{R}(\xi; q) - C\xi. \tag{15}$$

Since $\partial/\partial\xi\ R(\xi, q)$ is a strict monotonic and continuous function in ξ, we will find for each C and q a unique $\xi^*(C, q)$ with

$$\left.\frac{\partial}{\partial \xi} F(\xi, C, q)\right|_{\xi = \xi^*(C,q)} = 0. \tag{16}$$

The points of stationary phase will be calculated by

$$\xi^*(C, q) = \left[\frac{\partial \tilde{R}(\xi; q)}{\partial \xi}\right]^{-1}(C). \tag{17}$$

In the next step, these points of stationary phase $\xi^*(C, q)$ are inserted into (15). Then, the stationary phase term is given by

$$\Psi(k_r, C, q) = -k_r G(C, q) \tag{18}$$

where $G(C, q) = F(\xi^*, C, q)$. Now, we can simplify (12) by applying the principle of stationary phase and obtain

$$Z(k_\xi, k_r) = \int e^{-jk_r G(C,q)} \bar{w}\left(\xi^*(C, q); q\right) \tilde{A}(k_\xi; q)dq \tag{19}$$

where $\bar{w}(\xi^*(C, q); q) = \alpha \tilde{w}(\xi^*(C, q); q)$. The amplitude factor α results from the integration in ξ.

E. Factorization

The properties of $G(C, q)$ determine whether the approximated kernel can be used to transform the imaging equations to a Fourier-based processor. We call the spatial invariant bistatic processing task separable if $G(C, q)$ is linear in $q : G(C, q) = g(C) + qh(C)$. If the task turns out to be separable, (19) can be further evaluated as follows:

$$\begin{aligned} Z(k_\xi, k_r) &= \int e^{-jk_r(g(C)+h(C)q)} \bar{w}(C, q)\tilde{A}(k_\xi; q)dq \\ &= e^{-jk_r g(C)} \int e^{-jk_r h(C)q} \bar{w}(C, q)\tilde{A}(k_\xi; q)dq. \qquad (20) \end{aligned}$$

The integral in (20) can be considered as the Fourier transform of $\tilde{A}(k_\xi; q)$ in the second variable including the window function $\bar{w}(C, q)$. The new defined wavenumber variable is

$$k_q = k_r h(C). \tag{21}$$

Then, we obtain from (20)

$$Z(k_\xi, k_r) = e^{-jk_r g(C)} \tilde{A}(k_\xi, k_q). \tag{22}$$

Solving (22) to the 2-D Fourier transform of the windowed data $\tilde{A}(k_\xi, k_q)$ and replacing C, we have

$$\tilde{A}(k_\xi, k_q) = e^{jk_r g(-k_\xi/k_r)} Z\left(k_\xi, \frac{k_q}{h(-k_\xi/k_r)}\right). \tag{23}$$

This means that the 2-D Fourier transform of the windowed data $\tilde{A}(k_\xi, k_q)$ can be recovered by interpolation of $Z(k_\xi, k_r)$ in the second variable and by multiplication with a phasor to remove the phase introduced by $g(C)$. In the last two steps, the reflectivity itself is reconstructed by the application of a 2-D inverse Fourier transform followed by resampling to the original xy domain.

F. Linear Approximation

A general linearization of $G(C, q)$ is not possible. In other words, an exact bistatic range migration processor as defined before does not exist even for the special case of an arbitrary spatial invariant problem. The stationary phase has to be evaluated numerically, and the function $G(C, q)$ has to be approximated by a linear fit.

One method to approximate G by a linear function is sketched in the following. First, we have to determine the mapping $y = f(q)$ in such a way that $G(C^*, q)$ is linear in q for a central C^*. This can be done by defining the function $\gamma(y) = G_0(C^*, y)$ in the original y domain and setting $f(q) = \gamma^{-1}(q)$. Then, $G(C^*, q) = G_0(C^*, f(q)) = q$, and the linearization for this fixed C^* is perfect with $g(C^*) = 0$ and $h(C^*) = 1$. Finally, for each other C, we have to interpolate $G_0(C, y)$ in the original y domain at the new points $f(q)$, so that we have $G_0(C, f(q))$ and fit this function by a straight line over the interesting q area. The results of the linear fits are the functions $g(C)$ and $h(C)$ depending on C.

The remaining errors can be controlled by dividing the frequency data into several separately processed segments. One way to perform such a multi-k segment processing is described in [2].

G. Monostatic Case

In the monostatic case, the linearization can be performed analytically. If h is the flight altitude, the range function is

$$R(\xi; y) = 2\sqrt{\xi^2 + h^2 + y^2}. \tag{24}$$

With $f(q) = \sqrt{q^2 - h^2}$, the phase function F yields

$$F(\xi, C, q) = 2\sqrt{\xi^2 + q^2} - C\xi \tag{25}$$

and the point of stationary phase can be resolved to

$$\xi^*(C, q) = q\frac{C}{\sqrt{4 - C^2}}. \tag{26}$$

Inserting (26) in (25), we have

$$G(C, q) = q\sqrt{4 - C^2}. \tag{27}$$

With $g(C) = 0$ and $h(C) = \sqrt{4 - C^2} = \sqrt{4 - (k_\xi^2/k_r^2)}$, the linearization in the monostatic case is proved.

If we proceed with the way described in the previous paragraph and choose $C^* = 0$, we have $\gamma(y) = 2\sqrt{h^2 + y^2}$ and

$$f(q) = \gamma^{-1}(q) = \sqrt{\left(\frac{q}{2}\right)^2 - h^2}. \tag{28}$$

With $G_0(C, y) = \sqrt{y^2 + h^2}\sqrt{4 - C^2}$ in the original y domain, we have

$$G(C, q) = G_0\left(C, f(q)\right) = q\sqrt{1 - \left(\frac{C}{2}\right)^2} \tag{29}$$

which again proves to be a successful linearization.

V. Range Migration by Using a Physical Reference

In the previous approach, our aim was to reconstruct the reflectivity in dependence on the new variable q by the numerical linearization of $G(C, q)$ in q. $G(C, q)$ was fitted by a straight line over the interesting q area.

For the spatial invariant case, it is also possible to use a physical reference to create an image [3]. Now, the variable q (in the following γ) gets the meaning of the bistatic semidistance. The new signal model is very similar to (10), i.e.,

$$Z(k_\xi, k_r) = \iiint e^{-jk_r(R_1(\xi';\gamma) + R_2(\xi';\gamma)) - jk_\xi(x + \xi')} \cdot a(x, \gamma)\, d\xi'\, dx\, d\gamma \tag{30}$$

where γ is the semibistatic distance, i.e.,

$$\gamma = \frac{R_1' + R_2'}{2}. \tag{31}$$

In this model, a point scatterer is referenced by elliptical coordinates $\mathbf{r} = (x, \gamma, \theta)$. The geometry is sketched in Fig. 3. For the further calculations and the application of the principle of stationary phase, we have to express R_1 and R_2 in (x, γ, θ), i.e.,

$$\begin{aligned} R_1^2 &= R_1'^2 + (\xi - x - x_I)^2 \\ R_2^2 &= R_2'^2 + (\xi - x + x_I)^2 \end{aligned} \tag{32}$$

and

$$\begin{aligned} R_1'^2 &= (\gamma + \gamma_I)^2 \\ R_2'^2 &= (\gamma - \gamma_I)^2 \end{aligned} \tag{33}$$

with $\gamma_I = (x_I/\gamma)r\,\cos\,\theta$, which can be approximated by the coordinates of the swath center γ_0, θ_0 and r_0. Then, γ_I can be calculated by $\gamma_I \approx (x_I/\gamma_0)r_0\,\cos\,\theta_0$.

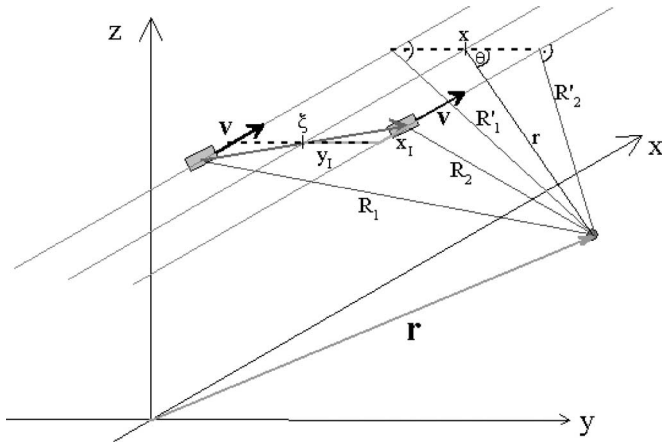

Fig. 3. Bistatic geometry for the approach in Section V.

Now, we want to solve the inner integral

$$I(k_\xi, k_r; x, \gamma) = \int e^{-jk_r(R_1(\xi';\gamma)+R_2(\xi';\gamma))-jk_\xi(x+\xi')} d\xi' \quad (34)$$

by applying the principle of stationary phase. For this, we rewrite this integral and use again the substitution $C = -k_\xi/k_r$. Equation (34) becomes

$$\begin{aligned} I(k_\xi, k_r; x, \gamma) &= \int e^{-jk_r(R_1(\xi';\gamma)+R_2(\xi';\gamma)-C\xi'-Cx)} d\xi' \\ &= \int e^{-jk_r(F(\xi',C,\gamma)-Cx)} d\xi' \end{aligned} \quad (35)$$

where

$$F(\xi', C, \gamma) = R_1(\xi';\gamma) + R_2(\xi';\gamma) - C\xi'. \quad (36)$$

In the next step, we have to find the point of stationary phase numerically similar to (16) by using (32) and (33). If ξ'^* is the point of stationary phase, (35) can be simplified and is given by

$$\begin{aligned} I(k_\xi, k_r; x, \gamma) &= \alpha e^{-jk_r(F(\xi'^*,C,\gamma)-Cx)} \\ &= \alpha e^{-jk_r\psi(C,x,\gamma)} \end{aligned} \quad (37)$$

where α is a coefficient that is supposed to be constant. To compute (30) by a 2-D inverse Fourier transform, we have to rewrite ψ, i.e.,

$$\psi(C, x, \gamma) = h_\gamma(C)\gamma + h_x(C)x + g(C). \quad (38)$$

Now, we have to evaluate $h_\gamma(C)$, $h_x(C)$, and $g(C)$ by developing the phase ψ about x_0 and γ_0, the center of swath, i.e.,

$$\begin{aligned} \psi(C, x, \gamma) \approx \psi(C, x_0, \gamma_0) &+ \frac{\partial\psi}{\partial x}(C, x_0, \gamma_0)(x - x_0) \\ &+ \frac{\partial\psi}{\partial\gamma}(C, x_0, \gamma_0)(\gamma - \gamma_0). \end{aligned} \quad (39)$$

In [3], it is shown that we have

$$\begin{aligned} g(C) &= F\left(\xi'^*(C, \gamma_0), C, \gamma_0\right) - h_\gamma\gamma_0 \\ h_x &= -C \\ h_\gamma &= \frac{\gamma_0 + \gamma_I}{\sqrt{(\gamma_0+\gamma_I)^2+(\xi'^*-x_I)^2}} + \frac{\gamma_0 - \gamma_I}{\sqrt{(\gamma_0-\gamma_I)^2+(\xi'^*+x_I)^2}}. \end{aligned} \quad (40)$$

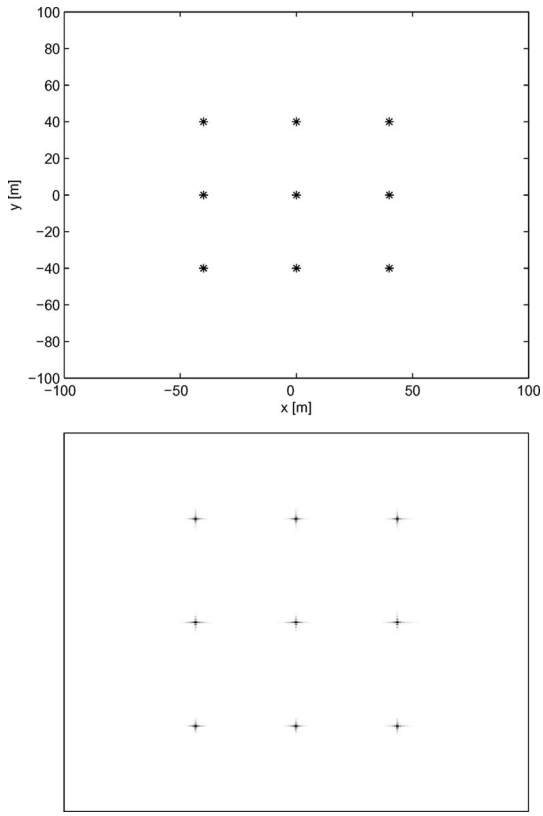

Fig. 4. Simulated scene and processed image with the bistatic range migration processor.

Finally, we can rewrite (30), so that it can be solved by a 2-D inverse Fourier transform, i.e.,

$$\begin{aligned} Z(k_\xi, k_r) &= \iint \alpha a(x, \gamma) e^{-jk_r(h_\gamma(C)\gamma - Cx + g(C))} dx\, d\gamma \\ &= \alpha e^{-jk_r g(C)} \iint a(x, \gamma) e^{-jk_r h_\gamma(C)\gamma - jk_\xi x} dx\, d\gamma \\ &= \alpha e^{-jk_r g(C)} A\left(k_\xi, k_r h_\gamma(C)\right). \end{aligned} \quad (41)$$

VI. Simulation

A raw data simulator was written to verify the bistatic range migration algorithm presented in Section IV. The simulator is able to produce the raw data for various point targets. A simulated scene with nine point reflectors and the reconstructed scene is shown in Fig. 4. The assumed platform parameters are summarized in Table I. The complete range migration processing consists of the following steps.

- Transform data to (k_ξ, k_r) domain.
- Determine the mapping $y = f(q)$ in such a way that $G(C^*, q)$ is linear in q for a central C^*.
- For each C, q, calculate $G(C, q)$ and fit this function by a straight line in the q variable by $g(C) + h(C)q$.
- Develop the image in the (k_ξ, k_q) domain by interpolation and multiplication by a phasor.
- Apply a 2-D inverse Fourier transform to the (k_ξ, k_q) domain and resample the image to the xy plane.
- Repeat the process for different segments if the introduced phase error is too large.

TABLE I
SIMULATION PARAMETERS

Platform velocity	100 m/s
Center frequency	10 GHz
Bandwidth	300 MHz
Scene extent	200 m x 200 m
Across y-Tx/Rx separation	1050 m
Bistatic angle	14°

Fig. 5. Sensor platforms. (Top) Dornier Do-228 with AER-II and (bottom) Transall C-160 with PAMIR.

The simulation shows that the range migration algorithm works very well under ideal conditions. In practice, it is very important to reproduce the real bistatic range history to obtain the best results.

VII. FLIGHT EXPERIMENTS

Besides other radar research institutes [8], [9], the Forschungsgesellschaft für Angewandte Naturwissenschaften (FGAN) also undertook a bistatic airborne experiment with its two SARs, namely sensors AER-II and PAMIR, in October 2003 [10], [11].

The X-band SAR system AER-II [12] has been operating under FGAN since March 1996 onboard a Transall C-160. It allows to demonstrate several operational modes like moving target indication (MTI), interferometry, polarimetric SAR, and spotlight SAR. This is possible due to its active polarimetric phased array and its four receiving channels. The main antenna consists of (6×44) polarimetric patch elements and 16 transmit/receive (T/R) modules. The transmit peak power is about 80 W, and the signal bandwidth is 160 MHz. For the bistatic SAR experiments, the AER-II sensor was used only as transmitter and placed on a Dornier Do-228 (see Fig. 5). The transmit antenna was mounted in the floor of the aircraft fuselage. It was possible to rotate the antenna in such a way that incidence angles from $-40°$ to $40°$ were manually adjustable. The antenna has a 3-dB beamwidth in azimuth of about $3°$ and in elevation of about $15°$. The signal generation unit was replaced by an arbitrary waveform generator (AWG) to obtain

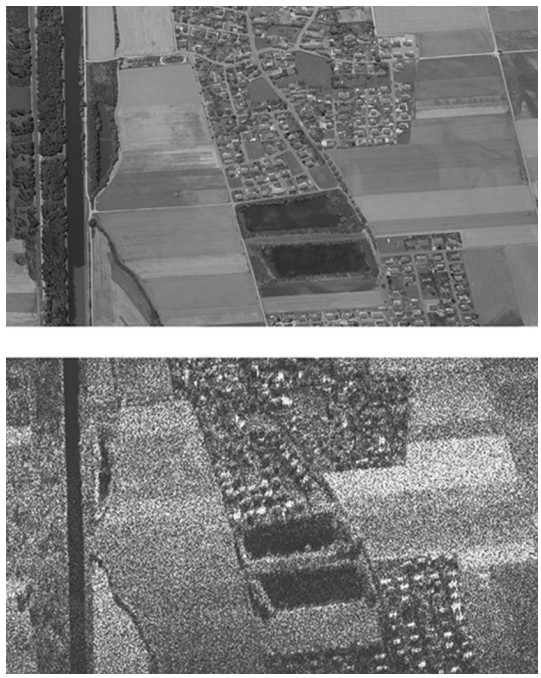

Fig. 6. Optical image (LVG Bayern) and bistatic SAR image (processed by the range migration algorithm) of Waltershoven, Germany.

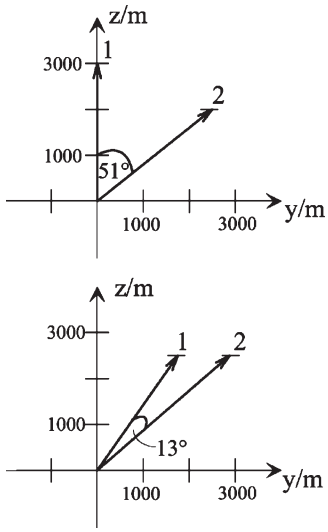

Fig. 7. Bistatic constellations (1, transmitter; 2, receiver) for the SAR images in Figs. 6 and 8.

a higher signal bandwidth of 300 MHz and a center frequency close to a PAMIR subband center frequency.

The receiving sensor PAMIR [13], which is the follow-up system of AER-II, has been operating under FGAN since August 2002 also onboard a Transall C-160 (see Fig. 5). PAMIR's important features are its multimode operation [strip, squinted strip, spotlight, sliding spotlight, SCAN MTI, inverse SAR (ISAR), and 3-D interferometric SAR (IfSAR)] and the ability to obtain SAR images with a very high spatial resolution. The total bandwidth amounts to 1.8 GHz and can be split into five subbands with 360 MHz each. Besides the electronical azimuth beam steering, the antenna has a mechanical elevation beam steering with depression angles up to $40°$. During the bistatic experiments, PAMIR received the echoes

Fig. 8. Optical image (LVG Bayern) and bistatic SAR image (processed by a time-domain algorithm) of Oberndorf, Germany.

from the AER system in one subband and stored the data to a fiber channel disk array.

A real synchronization of the oscillators was not possible because no data link between the platforms was installed. To overcome this problem, we choose a very large receiving window and a high transmitter PRF, which was a multiple integer of the receiver PRF of 1250 Hz. Then, the length of the receiving window was adapted in such a way that at least the echoes of one pulse were recorded.

In all flight configurations, the two aircrafts flew in a translational invariant configuration. The overlap of the antenna footprints was only guaranteed by careful flight planning and pilots' skill. Both sensors use a GPS/differential GPS (DGPS) system to obtain a precise trajectory of the platforms. Primarily, the influence of the bistatic angle was explored. For this purpose, the distance and the altitudes of the airplanes were adjusted, resulting in bistatic angles of 13°, 29°, 51°, and 76°. To the authors' knowledge, these are the first experiments with such large bistatic angles and a signal bandwidth of 300 MHz.

Fig. 6 shows a bistatic SAR image processed with the described range migration processor. The value of the bistatic angle was about 51°, and with considerations of the sensor positions and the signal bandwidth, we obtain the finest theoretical ground range resolution of about 1.30 m [14]. The positions of the platforms are shown in Fig. 7. The image quality can still be increased by applying motion compensation, which will be the next step. Fig. 8 shows the result of a time-domain-based image formation. Here, the inversion of (6) is done by means of a 2-D space-variant matched filtering, which is an optimal solution to the given integral equation [15]. Due to nonideal carrier tracks, a motion compensation step based on phase tracking of prominent scatterers had to be performed first. This image was acquired in a bistatic constellation, where the bistatic angle is about 13° and the finest theoretical ground range resolution is about 0.76 m (see Fig. 7).

VIII. Conclusion

In this paper, a bistatic range migration processor for the translational invariant case was presented. We have shown two different ways to linearize the phase function. The first approach is based on a linear fit of an exponential term, and the second approach uses a Taylor series to linearize the exponential term. Phase correction and resampling functions have—in contrary to the monostatic range migration algorithm—to be calculated numerically. The remaining errors can be controlled by dividing the frequency data into several separately processed segments. It should be mentioned that this kind of range migration processor passes into the optimum processor for any of the following limits:

- swathwidth-to-range ratio tends to zero;
- relative bandwidth tends to zero;
- bistatic angle tends to zero.

Furthermore, the bistatic range migration algorithm was tested successfully with simulated and real bistatic data.

Acknowledgment

The authors would like to thank the Bundeswehr Technical Center WTD 61 for the performance of the flight trials.

References

[1] M. Soumekh, "Bistatic synthetic aperture radar inversion with application in dynamic object imaging," *IEEE Trans. Signal Process.*, vol. 39, no. 9, pp. 2044–2055, Sep. 1991.

[2] J. Ender, "A step to bistatic SAR processing," in *Proc. EUSAR*, Ulm, Germany, May 2004, pp. 359–363.

[3] V. Giroux, H. Cantalloube, and F. Daout, "An omega-k algorithm for SAR bistatic systems," in *Proc. IGARSS*, Seoul, Korea, Jul. 2005, pp. 1060–1063.

[4] I. Walterscheid, J. Ender, A. Brenner, and O. Loffeld, "Bistatic SAR processing using an omega-k type algorithm," in *Proc. IGARSS*, Seoul, Korea, Jul. 2005, pp. 1064–1067.

[5] D. D'Aria, A. M. Guarnieri, and F. Rocca, "Precision bistatic processing with a standard SAR processor," in *Proc. EUSAR*, Ulm, Germany, May 2004, pp. 385–388.

[6] O. Loffeld, H. Nies, V. Peters, and S. Knedlik, "Models and useful relations for bistatic SAR processing," *IEEE Trans. Geosci. Remote Sens.*, vol. 42, no. 10, pp. 2031–2038, Oct. 2004.

[7] J. Ender, "The meaning of k-space for classical and advanced SAR-techniques," in *Proc. PSIP*, Marseilles, France, Jan. 2001, pp. 23–28.

[8] G. Yates, A. M. Horne, A. P. Blake, R. Middleton, and D. B. Andre, "Bistatic SAR image formation," in *Proc. EUSAR*, Ulm, Germany, May 2004, pp. 581–584.

[9] M. Wendler, G. Krieger, R. Horn, B. Gabler, and P. Dubois-Fernandez, "Results of a bistatic airborne SAR experiment," in *Proc. Int. Radar Symp.*, Dresden, Germany, Oct. 2003, pp. 247–253.
[10] I. Walterscheid, A. Brenner, and J. Ender, "Geometry and system aspects for a bistatic airborne SAR-experiment," in *Proc. EUSAR*, Ulm, Germany, May 2004, pp. 567–570.
[11] J. Ender, I. Walterscheid, and A. Brenner, "New aspects of bistatic SAR: Processing and experiments," in *Proc. IGARSS*, Anchorage, AK, Sep. 2004, pp. 1758–1762.
[12] L. Rössing and J. Ender, "The multi-channel SAR system "AER-II"—State of the program and new results," in *Proc. GRS*, Berlin, Germany, Oct. 2000, pp. 47–52.
[13] A. Brenner and J. Ender, "Demonstration of advanced reconnaissance techniques with the airborne SAR/GMTI sensor PAMIR," in *Proc. Inst. Elect. Eng., Radar, Sonar, Navig.*, Apr. 2006, vol. 153, pp. 152–162.
[14] I. Walterscheid, A. Brenner, and J. Ender, "New results on bistatic synthetic aperture radar," *Electron. Lett.*, vol. 40, no. 19, pp. 1224–1225, Sep. 2004.
[15] A. Brenner, "Distributed SAR processing in the time domain," in *Proc. EUSAR*, Cologne, Germany, Jun. 2002, pp. 573–576.

Ingo Walterscheid received the Diploma degree in electrical engineering from the University of Siegen, Siegen, Germany, in 2002.

Since July 2002, he has been a Research Associate with the Research Institute for High Frequency Physics and Radar Techniques (FHR), Forschungsgesellschaft für Angewandte Naturwissenschaften (FGAN), Wachtberg, Germany. His current research interests are in the areas of bistatic SAR systems and experiments, monostatic and bistatic SAR signal theory, and bistatic SAR processing.

Mr. Walterscheid is a member of the International Postgraduate Programme "Multi Sensorics" at the Center for Sensorsystems (ZESS), University of Siegen.

Joachim H. G. Ender (M'94–SM'06) received the degree in mathematics and physics from the University of Muenster, Muenster, Germany, and the Ph.D. degree in electrical engineering from the Ruhr-University Bochum, Bochum, Germany.

In 1976, he joined the German defense research establishment Forschungsgesellschaft für Angewandte Naturwissenschaften (FGAN), where he worked on the statistical theory of detection and estimation, phased array antennas, imaging radar, radar signal processing problems, and design and construction of airborne experimental radar systems. In 2005, he became a Principal Investigator for a hybrid bistatic SAR experiment between the radar satellite TerraSAR-X and the airborne SAR system Phased Array Multifunctional Imaging Radar. Since 1992, he has been lecturing on radar techniques and signal processing with the Ruhr-University Bochum. Since 2005, he has been teaching at the Technical University RWTH-Aachen, Aachen, Germany. He is currently the Director of the Research Institute for High Frequency Physics and Radar Techniques (FHR), FGAN, where he is responsible for research activities in various themes of radar and radar countermeasures. Furthermore, he serves as a Consultant on radar topics to government and industry and is engaged in academic education. He is the author or coauthor of numerous papers and frequently serves as a referee for various international journals and conferences. His current research interests include architectures of phased array antennas, multibaseline and wideband processing techniques for across-track SAR interferometry, ground moving-target detection with air- and space-based radar, inverse SAR for moving-target imaging, and bistatic SAR processing.

Dr. Ender is one of the Founder Members of the European Conference on Synthetic Aperture Radar, which started in 1996 and takes place every two years. He is a Member-at-Large of the Sensor and Electronics Technology Panel, NATO Research and Technology Organization; and a Member of the ITG/VDE and DGON. He is the Speaker of the Scientific Board and a Member of the Scientific Council of the International Postgraduate Programme for the Center of Sensorsystems (ZESS), University Siegen, Siegen, Germany. He received the Honorary Professor Award from the Ruhr-University Bochum in 2002.

Andreas R. Brenner received the Diploma degree in physics from the University of Karlsruhe, Karlsruhe, Germany, in 1987, and the Ph.D. degree in electrical engineering from the University of Aachen, Aachen, Germany, in 1993. His Ph.D. dissertation focused on the various problems in signal processing and image formation in the fields of magnetic resonance imaging and ultrasonic imaging.

In 2000, he joined the Institute for High Frequency Physics and Radar Techniques (FHR), Forschungsgesellschaft für Angewandte Naturwissenschaften (FGAN), Wachtberg, Germany. Since 2003, he has been the Head of the Array-Based Radar Imaging department. His current research interests include array-based radar imaging, multidimensional radar imaging, ultrahigh-resolution SAR, motion compensation, autofocusing methods, digital beamforming, and bistatic and multistatic radar imaging.

Otmar Loffeld (M'05–SM'06) received the Diploma degree in electrical engineering from the Technical University of Aachen, Aachen, Germany, in 1982, and the Eng. Dr. and Habilitation degrees in the field of digital signal processing and estimation theory from the University of Siegen, Siegen, Germany, in 1986 and 1989, respectively.

In 1991, he was appointed as a Professor for digital signal processing and estimation theory with the University of Siegen. Since then, he has given lectures on general communication theory, digital signal processing, stochastic models and estimation theory, and SAR. In 1995, he became a member of the Center for Sensorsystems (ZESS), which is a central scientific research establishment at the University of Siegen. Since 2005, he has been the Chairman of that Center. In 1999, he became a Principal Investigator (PI) on baseline estimation for the X-band part of the Shuttle Radar Topography Mission, where ZESS contributed to the German Aerospace Center's baseline calibration algorithms. He is a PI for interferometric techniques in the German TerraSAR-X mission, and, together with Prof. Ender from FGAN, he is one of the PIs for a bistatic spaceborne airborne experiment, where TerraSAR-X will serve as the bistatic illuminator, while FGAN's Phased Array Multifunctional Imaging Radar system mounted on a Transall airplane will be used as a bistatic receiver. Since 1991, 25 doctoral students completed their Ph.D. degrees under his supervision, and 25 Ph.D. students were cosupervised by him. In 2002, he founded the International Postgraduate Programme (IPP) "Multi Sensorics," which is a three-year doctoral degree course at the University of Siegen hosted by ZESS. Since 2002, he has been the Speaker of that programme, which by now comprises 25 international and 15 German doctoral students. He is the University's Scientific Coordinator for "Multidimensional and Imaging Systems," and furthermore, he is the Speaker and Coordinator of the University's research proposal "Environment Exploration NRW (E^2N)" in the Excellence Initiative promoted by the Federal Government of Germany. He is the author of two textbooks on estimation theory. His current research interests comprise multisensor data fusion, Kalman filtering techniques for data fusion, optimal filtering and process identification, SAR processing and simulation, SAR interferometry, phase unwrapping, and baseline estimation. His recent field of interest is bistatic SAR processing.

Prof. Loffeld is a member of the ITG/VDE. He received the Scientific Research Award of Northrhine-Westphalia (*Bennigsen-Foerder Preis*) for his works on applying Kalman filters to phase estimation problems such as Doppler centroid estimation in SAR as well as phase and frequency demodulation.